TRIBOLOGICAL BEHAVIOUR OF CROSS-SHAPED DIMPLES ON SLIDING SURFACES UNDER HYDRODYNAMIC LUBRICATION

Hardik GANGADIA*, **Saurin SHETH****

Research Scholar, Gujarat Technological University, Ahmedabad, Gujarat, India
**Mechatronic Engineering Department, G. H. Patel College of Engineering & Technology, V. V. Nagar, Gujarat, India

hgangadia@gmail.com, saurinsheth@gcet.ac.in

Abstract: This study reports on the tribological behaviour of sliding surfaces having cross-shaped micro-dimples on a surface. One wall is smooth and moving at a constant speed against the other fixed wall with dimples. The laser machine helps to create the desired dimples on the surface of the fixed wall. For the purpose of generating hydrodynamic pressure and tribological behaviour, the effects of cross-shaped dimples and oriented cross-shaped dimples have been compared with circular-shaped dimples. Additionally, the impact of sliding speed, dimple area density and depth on tribological behaviour was examined. The findings show that compared with a circular-shaped dimple, an unconventional cross-shaped and orientated cross-shaped dimple generates a higher net hydrodynamic pressure in the fluid domain and offers superior stability between the sliding surfaces. It has been demonstrated that geometrical factors like dimple depth and area density as well as operational factors like sliding speed have a substantial impact on the hydrodynamic average pressure and tribological behaviour of sliding surfaces. The experimental findings indicate that, for the same geometric and operating parameters, cross- and orientated cross-shaped dimples have a 20%–25% lower friction coefficient between the sliding surfaces than circular dimples. The results of the experiment support those of the analysis and CFD.

Key words: surface texturing, tribology, hydrodynamic lubrication, sliding surfaces, CFD, LST

1. INTRODUCTION

Hydrodynamic lubrication between sliding surfaces in components such as journal bearings and mechanical seals plays a significant role in improving the sliding surface tribological behaviour. Many studies have been conducted to improve the hydrostatic and hydrodynamic load capacity of sliding surfaces. Researchers have discovered that coning, misalignment, waviness and hydropads produce positive pressure and increase the load capacity of sliding surfaces [1–6].

Laser texturing has grown as a proven method in mechanical components over the past two decades. When one of the sliding surfaces is texturised, there is a rise in hydrodynamic pressure and load-carrying capacity, as well as a reduction in generated friction and wear. Many locales are now using surface texturing to get tribological benefits. Surface texturing techniques such as shot blasting [7], laser texturing [8, 9], reactive ion etching [10] and micro-electrolytic etching [11] are now widely available. When compared with other technologies, laser texturing provides unparalleled control of the surface microstructure while having a low environmental impact.

When the upper surface slides, the fluid is pushed forward by the relative motion of the sliding surfaces. When the fluid enters the dimple as it flows forward, the pressure reduces owing to diverging action, and as it moves out of the dimple, the pressure rises due to converging action. This difference in pressure drop and pressure rise results in net positive pressure creation, which enhances the load-carrying capacity between the sliding surfaces.

Etsion and Burstein [12] introduced a mechanical seal model with a hemispherical regular micro-surface on one of the mating seal faces, resulting in improved seal performance in terms of lower friction. According to Etsion et al. [13, 14], optimal pore depth over pore diameter maximises fluid film stiffness in laser textured surfaces. So far, the investigation has primarily concentrated on circular micro dimples [12–16] because of their ease of fabrication. Some researchers concentrated on conventionally shaped micro dimples such as square, triangle and ellipse [17–20], while others [18, 19] discovered that an elliptical dimple placed perpendicular to the direction of sliding produced the best load-carrying capacity results. Qui et al. [21] optimised the texture geometry and density of six different dimple shapes for maximum load-carrying capacity in the case of gas-lubricated parallel sliding bearings, concluding that the ellipsoidal dimple shape results in the highest load-carrying capacity and discovering that optimal geometry and density are almost independent of operating conditions. Following that, Qui et al. [22] adjusted the texture geometry and density of six alternative dimple shapes in terms of least friction coefficient and maximum bearing stiffness, reporting that the ellipsoidal shape yielded the lowest friction coefficient and the highest bearing stiffness. According to Raeymaekers et al. [23] and Yan et al. [11], dimple area density is also an important characteristic that influences the tribological behaviour of sliding surfaces.

Researchers [24–27] are now using commercial CFD programmes like FLUENT to compute the pressure and velocity distribution characteristics of lubricant flow between textured sliding surfaces. Recently, Liu et al. [26] used numerical simulation to study the geometry and operating parameters of spherical micro dimples on the tribological performance of textured surfaces

Hardik Gangadia, Saurin Sheth
Tribological Behaviour of Cross-Shaped Dimples on Sliding Surfaces Under Hydrody-Namic Lubrication

DOI 10.2478/ama-2024-0043

and recommended a dimple area density of 25%–35% in practical applications. Wei et al. [27] conducted a numerical analysis to determine the effect of geometric features on pressure build-up for various dimple shapes. This article also presented a new parameter called dimple surface angle, and it was discovered that the most significant changes occur when the dimple surface angle is <30°. Much study has been done to date to investigate the load-carrying capacity of one standard dimple shape (i.e. round, square, triangle, spherical, etc.) rather than the tribological characteristics of unconventional-shaped texturing. Non-traditional dimple shapes, on the contrary, have more potential for convergence and thus better tribological benefits than standard dimple shapes, which cannot be ignored. Gangadia and Sheth [28, 29] studied the effect of bowtie and star dimple shapes on circular dimple shapes to generate hydrodynamic pressure between two parallel sliding surfaces and found that when the sliding speed, area density and dimple depth are all the same, the oriented bowtie-shaped dimple produces the most hydrodynamic pressure.

In this study, an analytical model is developed to estimate the hydrodynamic pressure generation for the application of laser textured mechanical seals, followed by CFD analysis, to explore the effect of straight and orientated cross-shaped dimples over circular-shaped dimples. The experimental results matched well with the analytical method and CFD results. Coefficient of friction was examined for the parametric analysis to study the effect of different geometric characteristics such as dimple depth and dimple area density on hydrodynamic pressure. Operating parameters such as sliding speed are also covered.

2. ANALYTICAL MODEL

The geometrical model of laser textured mechanical seal is presented in Fig. 1. Inner and outer radii of the seal ring are ri and ro, respectively, and the values for the same has been taken as 0.0181 m and 0.0235 m, respectively. Each dimple is modelled by radius rd and depth HD. Laser textured dimples are distributed uniformly on one of the faces of seal. Each dimple is modelled at the centre of the imaginary square cell with length of 2r1 as shown in Fig. 1(c). Length of the imaginary square cell with relation to circular dimple area density Sp is as follows:

$$2r_1 = \sqrt{\frac{\pi}{S_d} \times r_d} \tag{1}$$
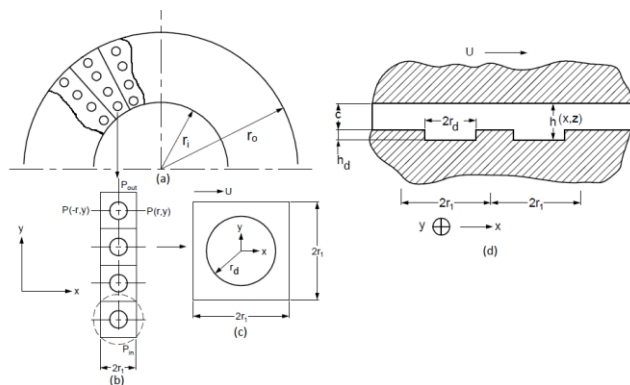

Fig. 1. (a) Geometric model of laser textured mechanical seal (b) Dimple column (c) Dimple cell (d) Cross-section of the textured seal

Fig. 1(d) shows the cross-section of the textured seal. One of the two surfaces of the seal is provided with a micro-texture and the other surface is flat. The flat surface moves with relative velocity U to the textured surface. The minimum distance between the bearing surfaces is indicated by c and the local distance is indicated by h(x, z), where x and z are Cartesian coordinates as shown in the Fig 1. It is assumed that seal faces are separated by incompressible viscous fluid.

The generalised Reynolds's equation for mechanical seal is expressed as:

$$\frac{\partial}{\partial x}\left(h^3 \frac{\partial p}{\partial x}\right) + \frac{\partial}{\partial z}\left(h^3 \frac{\partial p}{\partial z}\right) = 6\mu U \frac{\partial h}{\partial x} \tag{2}$$

Modified Reynold's equation in order to deal with cavitation is:

$$\frac{\partial}{\partial x}\left(K\beta h^3 \frac{\partial \xi}{\partial x}\right) + \frac{\partial}{\partial z}\left(K\beta h^3 \frac{\partial \xi}{\partial z}\right) = 6\mu U \frac{\partial(\xi h)}{\partial x} \tag{3}$$

Dimensionless Reynold's equation is as follows:

$$\frac{\partial}{\partial X}\left(KH^3 \frac{\partial \xi}{\partial X}\right) + \frac{\partial}{\partial Z}\left(KH^3 \frac{\partial \xi}{\partial Z}\right) = \Lambda \frac{\partial \xi H}{\partial X} \tag{4}$$

Only one radial column of dimples is taken for consideration as it is assumed that micro-dimples are evenly distributed. Boundary condition for one radial column is as shown in Fig. 1(b):

$$p(x, z = r_i) = p_{in}$$

$$p(x, z = r_o) = p_{out} \tag{5}$$

In this analysis the pressure distribution is assumed to be periodic in the direction of the circumference with the same period as the length of the imaginary square cell. Therefore, in the direction of the circumference, the periodic condition of the pressure is applied as:
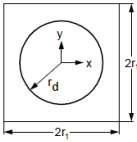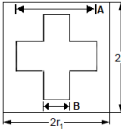
$$p(x = -r_1, z) = p(x = r_1, z) \tag{6}$$

Boundary conditions in dimensionless form are given as follows:

$$P\left(X, Z = \frac{r_i}{r_d}\right) = \frac{p_{in}}{p_a}$$

$$P\left(X, Z = \frac{r_o}{r_d}\right) = \frac{p_{out}}{p_a}$$

$$P\left(X = -\frac{r_1}{r_d}, Y\right) = P\left(X = \frac{r_1}{r_d}, Y\right) \tag{7}$$

Circular, cross and oriented cross-shaped dimples are considered in this study, which can be fabricated using LST. All dimples have flat bottoms and flat boundary walls and are symmetric to the XZ plane. Dimple-shaped geometry, the equivalent dimension of dimple with respect to area of circular dimple, cell size and dimensionless local spacing H(X,Y) between the textured and flat surface within one unit cell for cross shape dimple are described in Tab. 1.

Equation 3 can be solved for the pressure distribution in the seal clearance by a finite difference method with a relaxation factor of 1.4. Uniform Cartesian grid of 100 × 100 nodes is selected based on convergence and accuracy. The opening force to prevent contact between seal faces can be obtained by integrating the pressure over the seal area. SAE 30 oil was used in analysis and experimental work, which has dynamic viscosity of 0.29 kg/m/s at 20°C and density of 875 kg/m³.

Tab. 1. Details of all dimple-shaped geometries

Shape	Equivalent dimensions	Cell size	Conditions for film thickness H(X,Y)
Circular	$r_d = \sqrt{\dfrac{A_{circle}}{S_d}}$	$2r_1 = \sqrt{\dfrac{\pi}{S_d} \times r_d}$	$\begin{cases} 1 + \dfrac{\varepsilon}{\delta} & if\ X^2 + Y^2 \leq 1 \\ 1 & if\ X^2 + Y^2 > 1 \end{cases}$
Cross	$B = \sqrt{\dfrac{\pi}{5}} \times r_d$ And $A = 3B$	$2r_1 = \sqrt{\dfrac{5B^2}{S_d}}$	$\begin{cases} 1 + \dfrac{\varepsilon}{\delta} & if\ |X| \leq \dfrac{1}{\sqrt{10}}\ AND\ |Y| \leq \dfrac{3}{\sqrt{10}} \\ & or\ |Y| \leq \dfrac{1}{\sqrt{10}}\ AND\ |X| \leq \dfrac{3}{\sqrt{10}} \\ 1 & else \end{cases}$

3. CFD MODEL

CFD analysis has been done to reconfirm the results obtained from the analytical model prior to the experimental work. Fig. 1 (d) is reconstructed and shown as Fig. 2, which represents the geometric parameters of the CFD model. The length of the domain is denoted by $2r_1$ and it will remain constant for all the analyses. The quantity c is the fluid film thickness which is set in advance and quantity HD is the depth of the dimple.
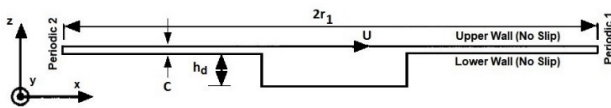

Fig. 2. Geometric parameters and boundary conditions of model

The fluid domain's boundary conditions are likewise depicted in the same Fig. 1(d). At both the upper and lower walls, fluid has no slip condition. A periodic boundary condition confines the edges in the *x*-direction. The bottom wall is stationary, while the upper wall with an untextured surface slides in the *x*-direction with constant velocity *U*. Fig. 3 depicts the design and modelling of circular, cross and oriented cross surface texturing shapes for hydrodynamic analysis.
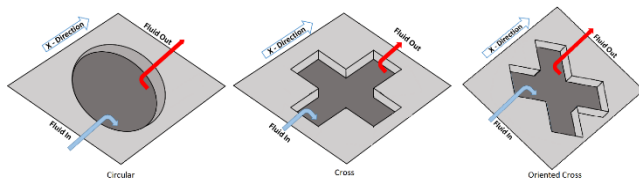

Fig. 3. Designs of dimple shapes

The lubricant is considered to be an incompressible Newtonian fluid with constant viscosity and density and no body force when filled between sliding pairs. The flow is described as laminar and isothermal. It is also believed that the effect of fluid pressure on the formation of a solid structure is insignificant. The flow of lubricant is governed by Navier–Stokes (momentum) equations and the continuity equation, which can be expressed as:

$$\rho(v.\nabla)v = -\nabla p + \nabla.(\mu \nabla v) \tag{8}$$

$$\nabla.v = 0 \tag{9}$$

The pressure distribution of lubricant between sliding pairs was estimated using the commercial CFD software FLUENT. The process for improving performance in creating hydrodynamic pressure in textured sliding surfaces is assumed to be connected to cavitation generation inside the dimples. In this case, the lubricant pressure may fall below the gas saturation pressure at the diverging zone, resulting in cavitation. The Rayleigh–Plesset multi-phase cavitation model [30], which has been successfully evaluated in references [31, 32], is employed. This is a multi-phase model in which lubricant vapour is created when the pressure drops below saturation. The results are obtained in dimensional form but given in nondimensional form to allow for easy comparison of different outcomes.

4. EXPERIMENTAL SET-UP

All of the experiments were carried out on a pin on disc wear testing machine, as indicated schematically in Fig. 4.
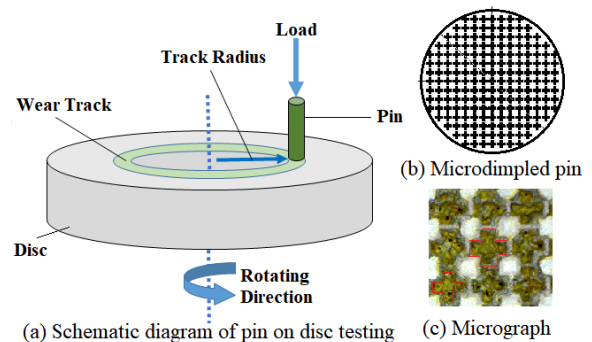

Fig. 4. Experimental set-up and specimen preparation (a) Schematic diagram of pin on disc testing (b) Microdimpled pin (c) Micrograph

The lower disc is fixed and can be rotated at any speed between 100 rpm and 2,000 rpm using a motor. The EN31 disc measures 165 mm in diameter and 8 mm in thickness. The textured pin is attached to a metallic holder that allows for vertical loading and self-alignment. SAE 30 oil is used as lubricating fluid. The mechanical assembly, base plate, guide base, AC motor, AC drive, spindle assembly, loading arrangement with pulley and 1:1

leverage ratio, loading pan with dead weights, wear disc holder, scale to set the track radius, LVDT for displacement and load cell for frictional force are the main components of the pin-on-disc wear testing apparatus. Sliding takes place between a rotating disc and a fixed pin. To fit the test conditions, the normal load and rotating speed can be changed. With the use of electronic sensors, frictional force and wear (displacement) are measured and recorded into a PC using Mag-view 2015 software. Software on the computer directly displays the value of the friction coefficient, which was calculated based on the magnitude of the frictional force. The sensor is affixed to the textured pin, which can measure the coefficient of friction. Data from sensors are acquired on a computer using an acquisition system.

4.1. Specimen preparation

The cylindrical textured pin measures 10 mm $\times$ 30 mm and 78.5 mm^2 in contact area with the disc. Cylindrical textured pins are made of EN31 steel with hardness of 45–50 HRC. Each pin was then polished and optically flattened before being examined for flatness with a monochromatic check light. A laser marking machine is used to texture the pins. A dimple drawing that meets the necessary dimensions is created and imported into the laser marking machine. The loop count is adjusted in accordance with the required depth, speed is set to 150 mm/s, power is set to 100% and frequency is set to 20 KHz. As illustrated in Fig. 4(b), micro-dimples are distributed evenly across the pin. Each trial began with the pins being cleaned with a cleaner and the weight of each pin being measured with a digital electronic weighing machine.

4.2. Test procedure

For the test first the textured pin was installed with a metallic holder and the flow of lubricant was started. Track radius is kept at 40 mm. After reaching a certain level of lubricant, the motor is started. The force sensor measures the friction force between the two samples by means of a piezoelectric (load cell) sensor as an acquisition mechanism. By dividing the normal force by the friction force produced in direct contact between the two surfaces as determined by a data collecting device, one can get the friction coefficient. Then the values of coefficient of friction were recorded for different speeds and loading conditions. When the test is over, the textured pin is replaced by a new one.

5. RESULTS AND DISCUSSION

More hydrodynamic pressure between the sliding surfaces results in a larger separation being maintained between them, which reduces friction. Greater tribological advantage and less friction are associated with increased hydrodynamic pressure. While the results of the experiments will be converted directly into a friction coefficient, the simulations will yield pressure as their output.

5.1. Effect of dimple shape

Fig. 5 illustrates the pressure distributions for a circular dimple, a cross dimple and a cross dimple positioned at 45°. All vari-

ables, such as sliding speed (U) = 6 m/s, dimple depth (h_p) = 15 m, dimple area density = 30% and fluid film thickness (c) = 2 μm, are held constant during the simulation for each shape to enable simple comparison. Fig. 5 shows that when the fluid flows along the x-axis and enters the dimple, the pressure drops owing to divergence initially. As the fluid travels forward, the pressure builds up due to the dimple's convergence, and this generated pressure is greater than the pressure decrease during divergence, resulting in a net positive pressure. Because all other geometric and operational parameters remain constant, the variation in net pressure is related solely to differences in dimple geometric shapes. However, geometric parameters such as dimple depth and area density, as well as operational parameters such as sliding speed, have a considerable role in the formation of hydrodynamic pressure.
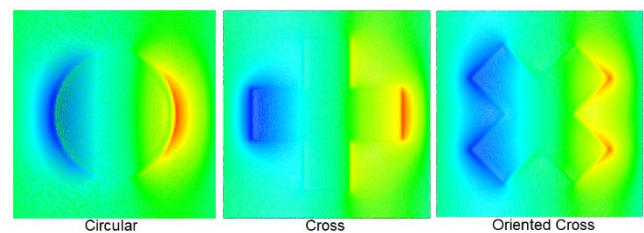

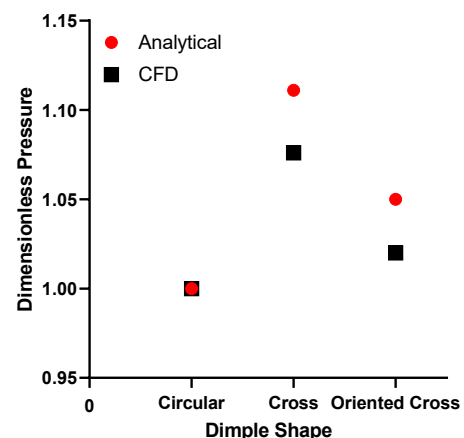**Fig. 5.** Pressure distribution in the fluid domain for different shapes

Fig. 6. Comparison of dimensionless average pressure

Fig. 6 compares dimensionless average pressures for the dimple shapes discussed in this paper. The graphic clearly shows a significant correlation between the results of the analytical investigation and the CFD study. Because of the significant convergence around the dimple's periphery, the cross-shaped dimple generates approximately 10% more hydrodynamic pressure than the circular-shaped dimple for the values of geometric and operating parameters mentioned above. In the case of an orientated cross-shaped dimple, pressure build-up is also high.

5.2. Effect of dimple depth

Fig. 7 depicts pressure distributions for minimum and maximum depth for cross dimples and oriented cross dimples. To conveniently capture the hydrodynamic effect of depth for cross

and oriented cross dimples, all other variables are maintained identical. Fig. 7 clearly shows that as dimple depth increases, the convergence becomes more concentrated in the case of both cross and orientated cross-shaped dimples.
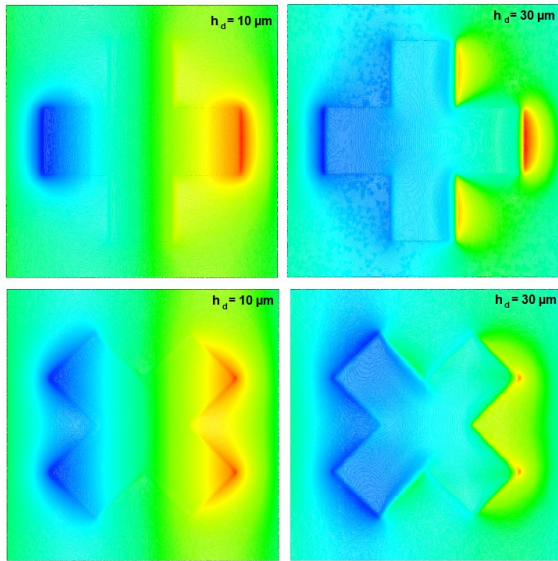

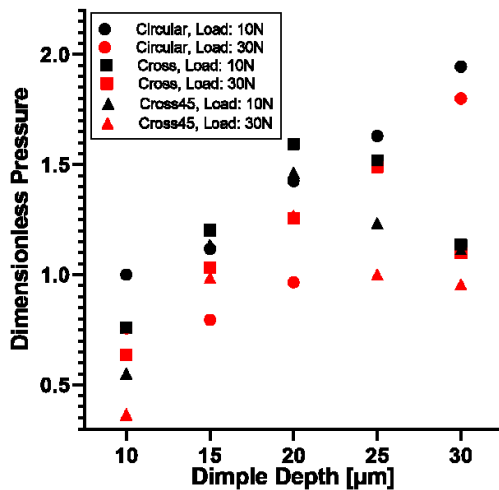**Fig. 7.** Pressure distribution in the fluid domain for different depths

Fig. 8. Dimensionless pressure as a function of dimple depth

Fig. 8 shows the dimensionless pressure as a function of dimple depth for two different loading conditions and dimple forms. In the case of circular dimples, the dimensionless pressure increases as the dimple depth grows. One way to think about it is that when the dimple depth increases, more lubricant gets trapped, which lubricates the sliding surfaces even more. Conversely, when the dimple depth increases, the lubricant undergoes a greater shear force, leading to the formation of micro-vortices. By narrowing the gap between the sliding surfaces and raising friction, these vortices may cause the lubricant to be sucked inward. In the case of cross and oriented cross dimples, dimensionless pressure increases as dimple depth grows from 10 µm to 20 µm and then drops as dimple depth climbs further. It is also discovered that cross dimples generate more pressure than circular dimples in the 15–20 µm dimple depth range. It is clear that dimple depth has an effect on the generation of hydrodynam-

ic pressure.

To understand the effects of dimple depth on tribological performance, the pressure distribution of the lubricant is analysed. Figs. 9–11 depict the pressure distribution of various dimple shapes along the *x*-direction at various depths, while Figs. 12–14 depict the pressure distribution of various dimple shapes along the *y*-direction at various depths. As the liquid enters the dimple, the pressure decreases and rises owing to convergence going in the *x*-direction.
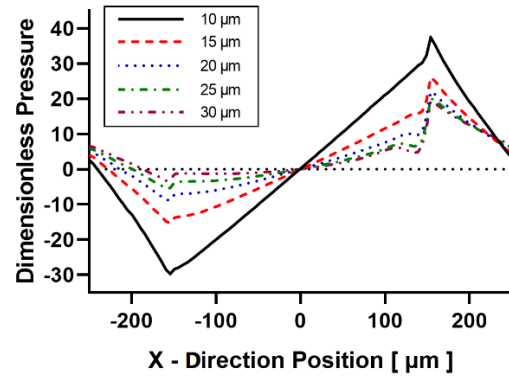

Fig. 9. Effect of dimple depth on pressure distribution along x-direction (for circular dimple)

The maximum magnitude of positive pressure is probably larger than the maximum magnitude of negative pressure. As a result of the net pressure rises, load-carrying capacity increases and friction reduces. The sliding surface's stability is dependent on how evenly the pressure is distributed. The stability of the sliding surface and the homogeneity of the pressure distribution increase with decreasing negative and positive pressure differential. Figs. 9–11 show that as the dimple depth increases, the difference between negative and positive pressure in the *x*-direction reduces and stability increases. It can also be seen that the pressure distribution in the *x*-direction is smoother in the case of oriented cross-shaped dimples, resulting in improved stability between the sliding surfaces. When discussing pressure distribution in the *Y*-direction, it can be seen in Figs. 12–14 that for each depth considered, approximate straight line of pressure distribution is observed in the case of cross-shaped dimples and two peaks of same level are seen in pressure distribution lines in the case of oriented cross-shaped dimples, and thus cross-shaped dimples and oriented cross-shaped dimples offer better stability than circular-shaped dimples between the sliding surfaces.
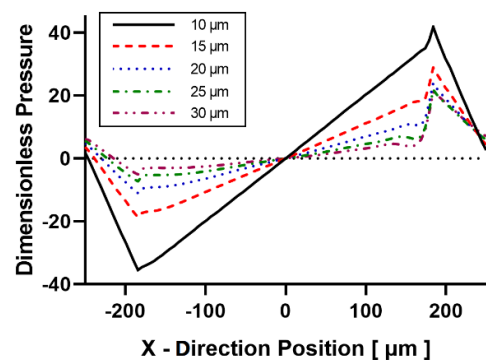

Fig. 10. Effect of dimple depth on pressure distribution along x-direction (for cross dimple)
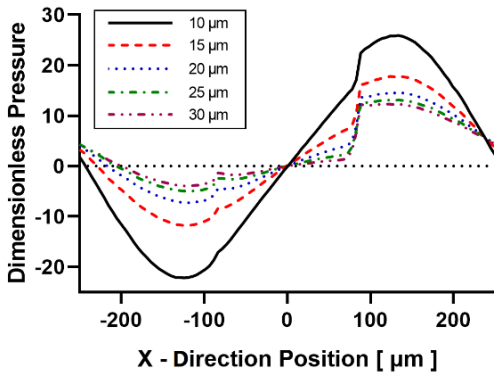
Hardik Gangadia, Saurin Sheth
Tribological Behaviour of Cross-Shaped Dimples on Sliding Surfaces Under Hydrody-Namic Lubrication

DOI 10.2478/ama-2024-0043

Fig. 11. Effect of dimple depth on pressure distribution along x-direction (for oriented cross dimple)
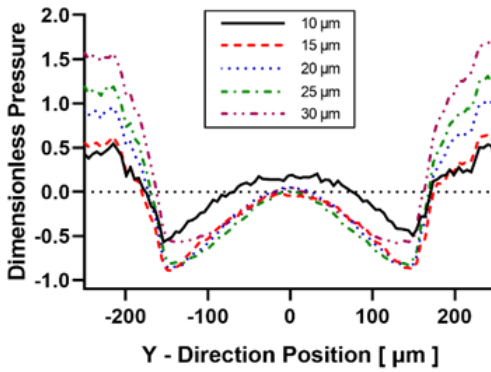

Fig. 12. Effect of dimple depth on pressure distribution along y-direction (for circular dimple)
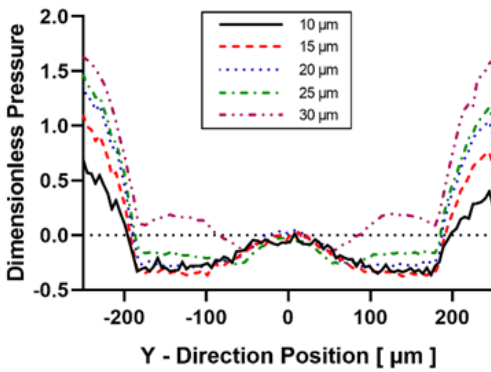

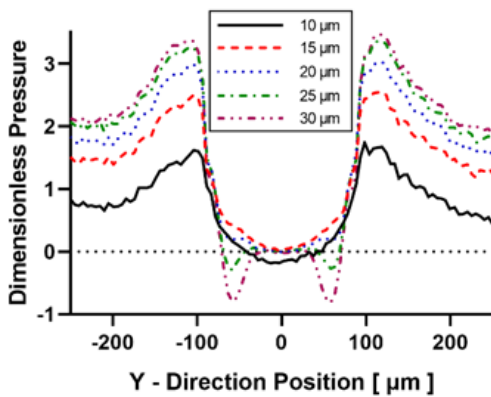**Fig. 13.** Effect of dimple depth on pressure distribution along y-direction (for cross dimple)

Fig. 14. Effect of dimple depth on pressure distribution along y-direction (for oriented cross dimple)

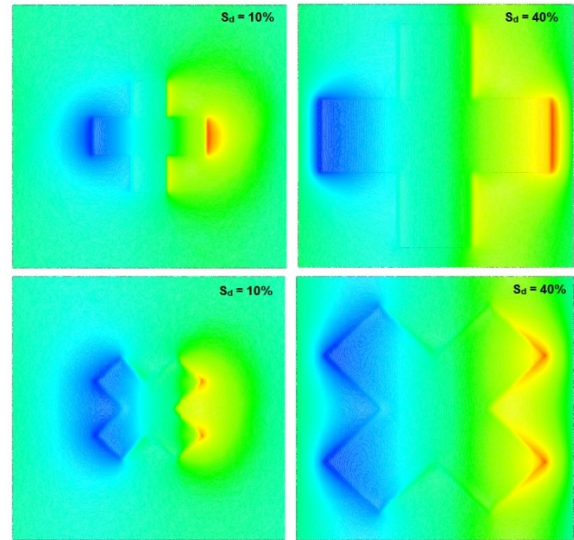### 5.3. Effect of dimple area density

Fig. 15. Pressure distribution in the fluid domain for different dimple area density

Fig. 15 shows pressure distributions for minimum and maximum dimple area density for cross dimple and oriented cross dimple. To conveniently capture the hydrodynamic effect of dimple area density for cross and oriented cross dimples, all other variables are held constant. The graphic clearly shows that when dimple area density increases, the amount of generating pressure decreases due to weaker convergence.
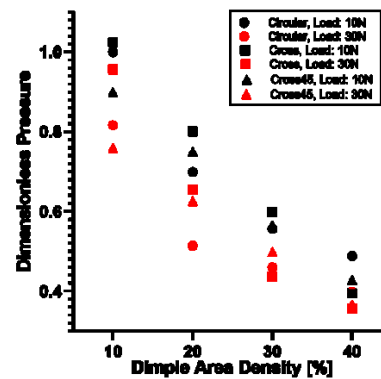

Fig. 16. Dimensionless pressure as a function of dimple area density

Fig. 16 depicts dimensionless pressure as a function of dimple area density for several dimple shapes under two different loading conditions. When the dimple area density is increased from 10% to 40%, the pressure declines steadily. Increasing the dimple area density could have a negative effect on the generation of hydrodynamic pressure. The shape of the dimple resembles a plane plate where micro hydrodynamic pressure is less likely to be generated when the dimple size is raised while the cell size stays constant. For a dimple area density of 10%, the pressure generated by a cross dimple is greater than the pressure generated by a circular dimple. The pressure generated by 20% and 30% dimple area density is greater than the pressure generated by circular dimple in both cross-shaped dimple and oriented cross-shaped dimple. When the dimple area density is increased

to 40%, circular dimples provide maximum pressure for both 10N and 30N loading conditions. It is obvious from this that modifying the dimple area density has a direct effect on the creation of hydrodynamic pressure.
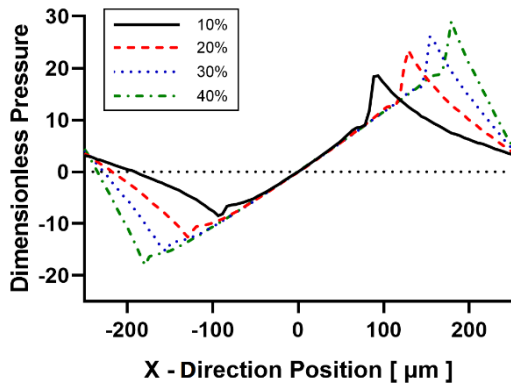
pressure decreases and the pressure rises owing to convergence going in the *x*-direction.

Fig. 17. Effect of dimple area density on pressure distribution along x-direction (for circular dimple)
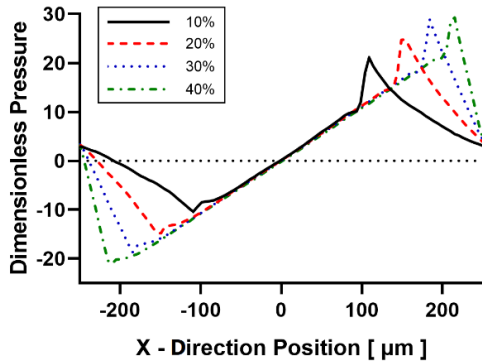

Fig. 18. Effect of dimple area density on pressure distribution along x-direction (for cross dimple)

Fig. 19. Effect of dimple area density on pressure distribution along x-direction (for oriented cross dimple)

Fig. 20. Effect of dimple area density on pressure distribution along y-direction (for circular dimple)

Fig. 21. Effect of dimple area density on pressure distribution along y-direction (for cross dimple)
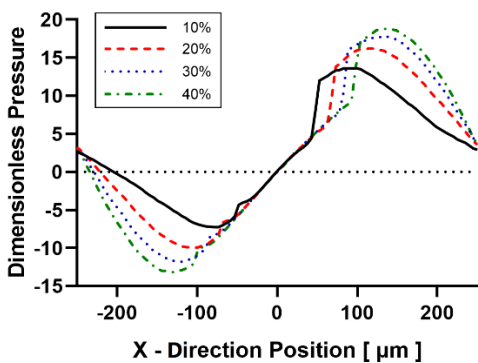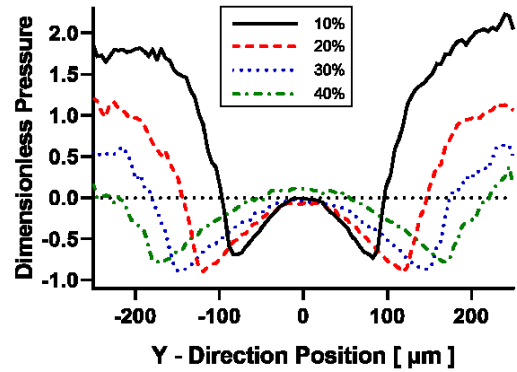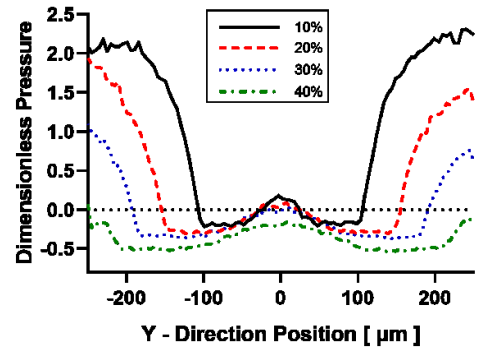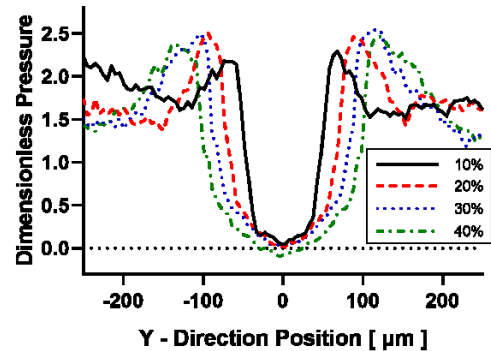

Fig. 22. Effect of dimple area density on pressure distribution along y-direction (for oriented cross dimple)

The lubricant's pressure distribution is studied in order to investigate the effects of dimple area density on tribological performance. Figs. 17–19 depict the pressure distribution of various dimple forms along the *x*-direction at various dimple area densities, while Figs. 20–22 depict the pressure distribution of various dimple shapes along the *y*-direction at various dimple area densities. As previously stated, as the liquid enters the dimple, the

The increase in net pressure can also be noticed here since the maximum magnitude of positive pressure is greater than the maximum magnitude of negative pressure. As a result, there is a tribological advantage between the sliding surfaces. Figs. 17–19 show that as dimple area density grows, so does the difference between negative and positive pressure in the *x*-direction. There is uniformity in the behaviour of circular dimples and cross-shaped dimples. However, when we talk about oriented cross dimples, the pressure distribution is more smooth and stable. When we look at the pressure distribution in the *Y*-direction, we

sciendo

Hardik Gangadia, Saurin Sheth
Tribological Behaviour of Cross-Shaped Dimples on Sliding Surfaces Under Hydrody-Namic Lubrication

DOI 10.2478/ama-2024-0043

can see that as the dimple area density grows from 10% to 40%, there is a little decrease in pressure for each form of dimple. The pressure distribution is more stable in the case of cross-shaped dimples than in the case of circular-shaped dimples and oriented cross dimples. Comparing Figs. 20 and 21, it is evident that the cross-shaped dimple improves the stability between the sliding surfaces by providing a more uniform pressure distribution at the centre than the circular dimple does. Over all the other scenarios evaluated, a cross-shaped dimple with 40% density provides the most stability.

5.4. Effect of speed

It has been demonstrated numerous times that the hydrodynamic pressure between sliding surfaces increases with increasing speed. However, if one of the sliding surfaces is textured, the hydrodynamic effects of speed on dimples of various shapes may differ. Fig. 23 illustrates the dimensionless pressure as a function of sliding speed for three different dimple shapes. Fig. 23 clearly shows that under both loading situations, there is little variation in the generated hydrodynamic pressure for all dimple forms analysed at a speed of 3 m/s, but this disparity grows as the speed increases.
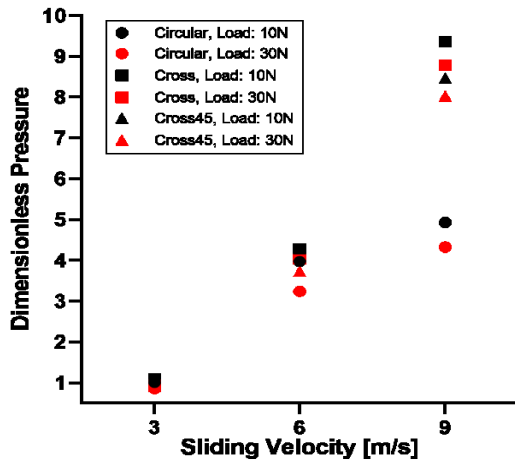
Fig. 23. Dimensionless pressure as a function of sliding speeds

Cross dimples and oriented cross dimples generate higher hydrodynamic pressure than circular dimples at 6 m/s, but the difference grows significantly larger at 9 m/s. The pressure created in the cross dimple is approximately 100% larger than the pressure generated in the circular dimple at a sliding speed of 9 m/s. Thus, using cross dimples as texturing rather than traditional circular dimples leads to a significant boost in hydrodynamic pressure generation and thus tribological benefits.

6. EXPERIMENTAL RESULTS

Fig. 24 represents the variation of the friction coefficient throughout several testing for circular, cross and orientated cross-shaped dimples. For each dimple shape, the dimple depth is set to 30 μm, the dimple area density is set to 40% and the RPM of the disc is set to 6 m/s sliding speed. The graph shows that the friction

coefficient for cross-shaped dimples and oriented cross-shaped dimples is substantially lower than the friction coefficient for circular-shaped dimples. As a result, cross-shaped and oriented cross-shaped dimples give better tribological advantages in sliding textured surfaces than traditional circular-shaped dimples.

Figs. 25–27 show the influence of dimple depth and density on average friction coefficient under uniform loading conditions for various dimple forms. Dimple depth is assumed to be 10 μm and 30 μm, and dimple area density is assumed to be 10% and 40%. As a result, four findings for three distinct speeds for each dimple shape are compared. As it can be seen, when rotational speed increases, the average friction coefficient drops. The lubricant film is created as a result of the rough surface, and film formation is easier at greater rotational speeds. The effect of dimple depth and dimple area density on tribological performance, on the other hand, appears to be significant.
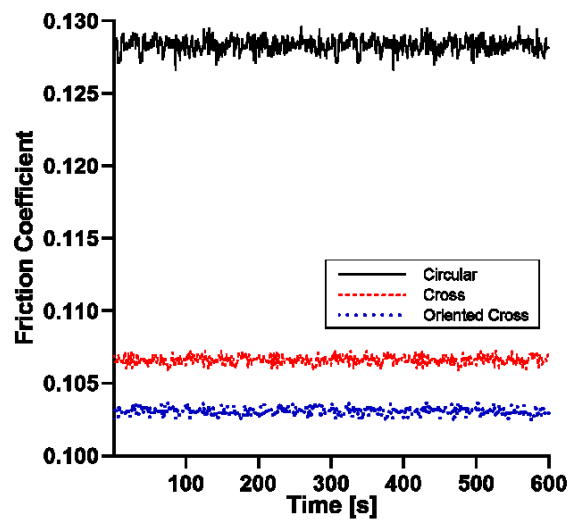
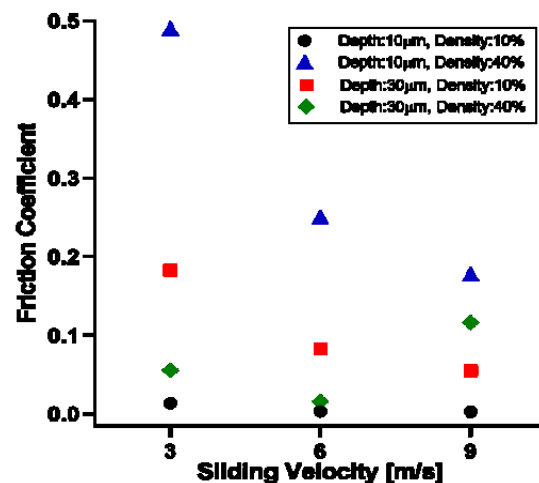**Fig. 24.** Variation of friction coefficient during different tests for different dimple shapes

Fig. 25. Friction coefficient as a function of sliding velocity for circular shaped dimple

Maximum friction coefficient is found for a combination of 10 μm dimple depth and 40% dimple area density at each speed and for each shaped dimple, and minimum friction coefficient is found

for a combination of 10 µm dimple depth and 10% dimple area density. Cross-shaped dimples have the lowest friction coefficient of all the shapes studied, with a velocity of 9 m/s for a combination of 10 µm dimple depth and 10% dimple area density. These experimental findings indicate a strong connection with the CFD and numerical model results.
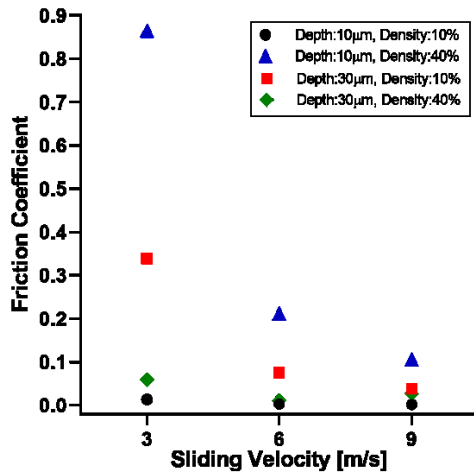

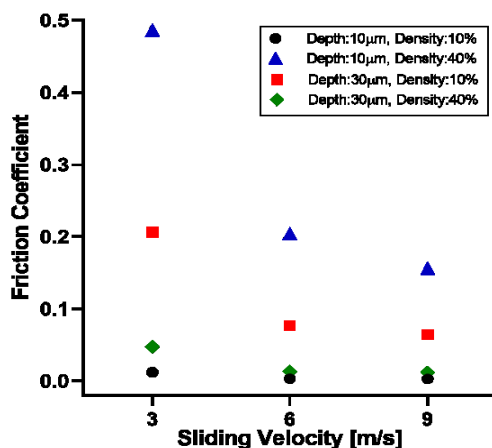**Fig. 26.** Friction coefficient as a function of sliding velocity for cross-shaped dimple

Fig. 27. Friction coefficient as a function of sliding velocity for oriented cross-shaped dimple

7. CONCLUSIONS

Using CFD and numerical models, it was found how cross and oriented cross dimple shapes affected the generation of hydrodynamic pressure between two parallel sliding surfaces. The tribological performance of textured samples with various types of dimples was then evaluated using pin on disc testing. The outcomes are listed below.

1. The cross-shaped dimple provides the most hydrodynamic pressure of the three dimple types when the dimple depth, dimple area density and sliding speed are all identical.
2. Dimple depth and area density have an effect on tribological behaviour and hydrodynamic pressure generation. Cross-shaped dimples and orientated cross-shaped dimples produce hydrodynamic pressure more effectively than circular dimples

for each dimple depth and dimple area density considered in the analysis.
3. The generated hydrodynamic pressure for all of the analysed dimple forms is about the same for all loading conditions at a speed of 3 m/s, but the discrepancies become more obvious as the speed increases. Cross-shaped dimples and oriented cross-shaped dimples produce greater hydrodynamic pressure than circular dimples at 6 m/s, but the difference becomes substantial at 9 m/s.
4. Cross-shaped dimples and oriented cross-shaped dimples provide more stability as pressure is distributed more evenly both in the x-direction and y-direction in the case of cross-shaped dimples and oriented cross-shaped dimples than it is in the case of circular-shaped dimples.
5. The shape of the dimple also has an effect on the friction coefficient. The test results accord well with those from the numerical and CFD models. The experimental findings indicate that, for the same geometric and operating parameters, cross- and orientated cross-shaped dimples have a 20%–25% lower friction coefficient between the sliding surfaces than circular dimples. The density and depth of dimples appear to have a substantial impact on tribological performance.
6. When used to obtain a tribological advantage on sliding surfaces under a variety of test load, dimple depth, dimple area density and rotational speed conditions, unconventional (cross or orientated cross)-shaped texturing outperforms traditional circular texturing.

It should be mentioned that there can be slight variations in the outcomes if the surface-to-surface contact is significant. To achieve the best response, surface textures' shape, orientation and geometric parameters can be optimised for particular applications and mechanical components.

REFERENCES

1. Haardt R., Godet M. Axial vibration of a misaligned radial face seal under a constant closure force. ASLE Trans, 1975;18: 55-61. https://doi.org/10.1080/05698197508982747
2. Etsion I. Squeeze effects in radial face seals. J. Lubric. Technol., 1980; 102: 145-152. https://doi.org/10.1115/1.3251452
3. Sharoni A., Etsion I. Performance of end-face seals with diametral tilt and coning-hydrodynamic effects. ASLE Trans, 1978; 24: 61-70. https://doi.org/10.1080/05698198108982998
4. Lebeck A. O., Teale J. L., Pierce R. E. Hydrodynamic lubrication and wear in wavy contacting face seals. J.Lubric. Technol, 1978; 100: 81-91. https://doi.org/10.1115/1.3453120
5. Ruddy A. V., Dowson D., Taylor C. M. The prediction of film thickness in a mechanical face seal with circumferential waviness on both the face and the seat. Journal of Mechanical Engineering Science, 1982; 24(1): 37-43.
   https://doi.org/10.1243/JMES_JOUR_1982_024_008_02
6. Key W. E., Salant R. F., Payvar P., Gopalakrishnan S., Vaghasia G. Analysis of a Mechanical Seal with Deep Hydropads. Tribology Transactions, 1989; 32(4): 481–489.
   https://doi.org/10.1080/10402008908981916
7. Nakano M, Korenaga A, Korenaga A, et al. Applying micro-texture to cast iron surfaces to reduce the friction coefficient under lubricated conditions. Tribol. Lett. 2007; 28: 131–137.
   https://doi.org/10.1007/s11249-007-9257-2.
8. Etsion I. State of the art in laser surface texturing. J. Tribol. 2005;127:248–253. https://doi.org/10.1115/1.1828070.

9. Voevodin A.A, Zabinski J.S. Laser surface texturing for adaptive solid

lubrication. Wear. 2006;261(11–12):1285–1292. https://doi.org/10.1016/j.wear.2006.03.013.

10. Wang X, Adachi K, Otsuka K, Kato K. Optimization of the surface texture for silicon carbide sliding in water. Appl. Surf. Sci. 2006;253(3):1282–1286. https://doi.org/10.1016/j.apsusc.2006.01.076.

11. Yan D, Qu N, Li H, Wang X. Significance of dimple parameters on the friction of sliding surfaces investigated by orthogonal experiments. Tribol. Trans. 2010;53:703–712. https://doi.org/10.1080/10402001003728889.

12. Etsion I, Burstein L. A model for mechanical seals with regular micro-surface structure. Tribol. Trans. 1996;39:677-683. https://doi.org/10.1080/10402009608983582.

13. Etsion I, Halperin G, Greenberg Y. Increasing mechanical seal life with laser-textured seal faces. In Proc. of 15th international conference on fluid sealing BHR group, Maastricht. 1997;3-11.

14. Etsion I, Kligerman Y, Halperin G. Analytical and experimental investigation of laser-textured mechanical seal faces. Tribol. Trans. 1999;42:511-516. https://doi.org/10.1080/10402009908982248.

15. Kligerman Y, Etsion I. Analysis of the hydrodynamic effects in a surface textured circumferential gas seal. Tribol. Trans. 2001;44(3):472-478. https://doi.org/10.1080/10402000108982483.

16. Etsion I, Halperin G. A laser surface textured hydrostatic mechanical seal. Tribol. Trans. 2002;45(3):430-434. https://doi.org/10.1080/10402000208982570.

17. Wang X.L, Hsu S.M. Integrated surface technology for friction control: A new paradigm effects of geometric shapes on friction. The 4th china international symposium on tribology. 2004;12-20.

18. Yu H, Wang X, Zhou F. Geometric shape effects of surface texture on the generation of hydrodynamic pressure between conformal contacting surfaces. Tribol. Lett. 2010;37:123-130. https://doi.org/10.1007/s11249-009-9497-4

19. Bai S, Peng X, Li Y, Sheng S. A hydrodynamic laser surface-textured gas mechanical face seal. Tribol. Lett. 2010;38(2):187-194. https://doi.org/10.1007/s11249-010-9589-1.

20. Yu H, Deng H, Haung W, Wang X. The effect of dimple shapes on friction of parallel surfaces. Proceedings of the institution of mechanical engineers, Part J: Journal of engineering tribology. 2011;225(8):693-703. https://doi.org/10.1177/1350650111406045.

21. Qiu M, Delic A, Raeymaekers B. The effect of texture Shape on the load-carrying capacity of gas-lubricated parallel slider bearings. Tribol. Lett. 2012;48:315–327. https://doi.org/10.1007/s11249-012-0027-4.

22. Qiu M, Minson B, Raeymaekers B. The effect of texture shape on the friction coefficient and stiffness of gas-lubricated parallel slider bearings. Tribology International. 2013;67:278-288. https://doi.org/10.1016/j.triboint.2013.08.004.

23. Raeymaekers B, Etsion I, Talke F.E. A model for the magnetic tape/guide interface with laser surface texturing. In proceedings of the ASME/STLE international joint tribology conference. 2008;669–671. https://doi.org/10.1115/IJTC2007-44173.

24. Han J, Fang L, Sun J, Ge S. Hydrodynamic lubrication of microdimple textured surface using three-dimensional CFD. Tribology Transactions. 2010;53:6:860-870. https://doi.org/10.1080/10402004.2010.496070.

25. Han J, Fang L, Sun J, Wang Y, Ge S, Zhu H. Hydrodynamic lubrication of surfaces with asymmetric microdimple. Tribology Transactions. 2011;54:4:607-615. https://doi.org/10.1080/10402004.2011.584364.

26. Liu W, Ni H, Chen H, Wang P. Numerical simulation and experimental investigation on tribological performance of micro-dimples textured surface under hydrodynamic lubrication. International Journal of Mechanical Sciences. 2019;163:105095. https://doi.org/10.1016/j.ijmecsci.2019.105095.

27. Wei Y, Tomkowski R, Archenti A. Numerical study of the influence of geometric features of dimple texture on hydrodynamic pressure generation. Metals, 2020;10:361. https://doi.org/10.3390/met10030361.

28. Gangadia H, Sheth S. Influence of the Bowtie Shaped Dimples on the Performance of Sliding Surfaces under Hydrodynamic Lubrication. Tribologia - Finnish Journal of Tribology. 2023; 40(1−2): 46−58. https://doi.org/10.30678/fjt.126885

29. Gangadia H, Sheth S. The Effect of Star Shaped Dimples on Sliding Surfaces under Hydrodynamic Lubrication, Tribology Online. 2023; 18(7): 457-468. https://doi.org/10.2474/trol.18.457

30. ANSYS Fluent Theory Guide, 2013.

31. Bakir F, Rey R, Gerber A. G, Belamri T, Hutchinson B. Numerical and experimental investigations of the cavitating behaviour of an inducer. Int. J. Totat. Mech. 2004; 10(1): 15-25. https://doi.org/ 10.1080/10236210490258034

32. Cupillard S, Glavatskih S, Cervantes M. J. Computational fluid dynamics analysis of a journal bearing with surface texturing. Proceedings of the Institution of Mechanical Engineers. Part J: Journal of Engineering Tribology. 2008; 222(2): 97-107. https://doi.org/10.1243/13506501JET319

Hardik Gangadia: iD https://orcid.org/0000-0002-7734-3402

Saurin Sheth: iD https://orcid.org/0000-0002-1792-7051